

Journal of Biomedical Optics

BiomedicalOptics.SPIEDigitalLibrary.org

Profiling of individual human red blood cells under osmotic stress using defocusing microscopy

Paula M. S. Roma
Livia Siman
Barbara Hissa
Ubirajara Agero
Erika M. Braga
Oscar N. Mesquita

SPIE.

Paula M. S. Roma, Livia Siman, Barbara Hissa, Ubirajara Agero, Erika M. Braga, Oscar N. Mesquita, "Profiling of individual human red blood cells under osmotic stress using defocusing microscopy," *J. Biomed. Opt.* **21**(9), 090505 (2016), doi: 10.1117/1.JBO.21.9.090505.

Profiling of individual human red blood cells under osmotic stress using defocusing microscopy

Paula M. S. Roma,^{a,*} Livia Siman,^a Barbara Hissa,^b Ubirajara Agero,^a Erika M. Braga,^c and Oscar N. Mesquita^a

^aUniversidade Federal de Minas Gerais, Departamento de Física, Avenida Antônio Carlos 6627, Belo Horizonte, Minas Gerais, Brazil

^bUniversity of Chicago, James Franck Institute, Institute for Biophysical Dynamics and Physics Department, Chicago, Illinois 60637, United States

^cUniversidade Federal de Minas Gerais, Departamento de Parasitologia, Avenida Antônio Carlos 6627, Belo Horizonte, Minas Gerais, Brazil

Abstract. We use a quantitative phase imaging technique, defocusing microscopy (DM), to measure morphological, chemical, and mechanical parameters of individual red blood cells (RBCs) immersed in solutions with different osmolalities. We monitor the RBCs' radius, volume, surface area, sphericity index, and hemoglobin content and concentration. The complete shape of cells is recovered and the effects of their adhesion to the glass substrate are observed. Finally, membrane fluctuation measurements give us information about the cells deformability. © 2016 Society of Photo-Optical Instrumentation Engineers (SPIE) [DOI: [10.1117/1.JBO.21.9.090505](https://doi.org/10.1117/1.JBO.21.9.090505)]

Keywords: optical microscopy; red blood cells; three-dimensional imaging; biomechanical properties.

Paper 160422LR received Jun. 17, 2016; accepted for publication Aug. 15, 2016; published online Sep. 21, 2016.

Changes in morphological, chemical, and mechanical parameters of red blood cells (RBCs) are known to be intimately related to many diseases.¹ In a routine blood examination, many RBCs' parameters, such as the mean corpuscular Hb content, mean corpuscular Hb concentration, mean corpuscular volume, and RBC distribution width (RDW), may be obtained and used as the main information to diagnose abnormalities in the cells. However, for a deeper understanding of the observed alterations, it is important to accurately access RBCs' properties at the single-cell level. In that sense, practical methods for the profiling of individual human RBCs are very desirable for both basic science and clinical use.

Some approaches to single RBC cell profiling using optical trapping, micropipette aspiration, atomic force microscopy, and microfluidics have been previously published.² However, none of them individually offer measurements of morphological, chemical, and mechanical indices of individual RBCs. Optical microscopy (OP) has shown to be a valuable tool to study

biomechanical parameters of cells, since it can be performed with minimal cell invasion and without the necessity of staining processes. Quantitative phase imaging (QPI) is an emerging field in OP developed for studying weakly scattering and absorbing objects, such as unlabeled cells. Recently, a QPI technique was applied to simultaneously characterize morphological, chemical, and mechanical parameters of individual RBCs.³ The technique presented here also returns morphological, chemical, and mechanical parameters, not simultaneously, but using a much simpler and practical setup.

Transparent objects (pure phase objects) that would be invisible when focused on a standard bright-field optical microscope can turn visible by simply defocusing the microscope. This occurs because the act of defocusing introduces a phase difference between the diffracted and nondiffracted orders generating image contrast. Defocusing microscopy (DM) is a QPI technique that uses defocus to observe phase objects like live unlabeled cells.^{4–10} From intensity images measured at two different focal positions, one can obtain the object's phase map and reconstruct the height profiles of each of its diffracting surfaces. In the case of an adhered red cell, the height profiles of the upper (free to fluctuate) and lower (adhered to the substrate) surface membranes are individually recovered. By surface membranes, we mean both plasma membrane and spectrin skeleton. The transport intensity equation,^{11,12} was previously used to retrieve quantitative phase images of the in-focus field from intensity images around the focus. However, this approach results in a differential equation that does not contain explicit phase terms that take into account the distance between the objective focal plane and the phase object diffracting surfaces, in a way that only the object's thickness profile is obtained and the complete characterization of all of its surfaces is not feasible.

In this work, the profiling of single RBCs under different osmotic conditions (200, 250, 300, 350, 400, and 450 mOsm/kg) was performed using DM and the cells' total 3-D shape, radius, volume, surface area, sphericity index (SI), Hb content, Hb concentration and membrane fluctuations were monitored. The methods used were derived from two DM measurements: intensity contrast (DMC) and mean square intensity contrast fluctuation (DMCF). Recently, DMC was used to obtain morphological parameters of RBCs related to retinal vascular disorders^{13,14} and submitted to different drug treatments.^{10,15,16} Furthermore, DMCF has been applied to retrieve cells membrane fluctuations and mechanical parameters.^{4,6,8,10}

Samples were prepared as described in Ref. 9. The NaCl concentrations were adjusted from 0.60% to 1.35% in order to obtain the desired osmolality. Experiments were performed using an inverted microscope (Nikon Eclipse TI-E, Nikon, Melville, New York) operating in bright-field mode and setup for Köhler illumination. The illumination was done with a halogen lamp (100 W) and the diffracted rays were collected by an oil immersion objective (Nikon Plan APO DIC H, 100X, NA 1.49; Nikon) [Fig. 1(a)]. Since RBCs strongly absorb light in the blue range of the visible spectrum,¹⁷ a long-pass filter (RF) was used allowing only the transmission of wavelengths above 610 nm. Images were captured with a CMOS camera (Silicon Video CMOS 642M, Epix Inc., Buffalo Grove, Illinois) at 326 frames per second. The defocus distance (z_f) was controlled and stabilized using Nikon Perfect Focus System (PFS Nikon). The defocus position $z_f = 0$ was set at the cell minimum contrast

*Address all correspondence to: Paula M. S. Roma, E-mail: paulamagda@ufmg.br

plane. Positive defocus positions ($z_f > 0$) were defined as the ones above the cell minimum contrast plane and negative defocus positions ($z_f < 0$) as the ones below it.

For the profiling of individual RBCs, 10 cells were imaged for 10 s at three different defocus positions z_f : $z_f = 0, 2,$ and $4 \mu\text{m}$ [Figs. 1(b)–1(d)]. The time mean intensity contrast $\langle C \rangle$ and time mean square intensity contrast fluctuation $\langle \Delta C^2 \rangle$ for each stack of images captured at a specific z_f were found by calculating, for each pixel, the following equations:

$$\langle C(\vec{\rho}, z_f) \rangle = \frac{\langle I(\vec{\rho}, z_f) \rangle - I_0}{I_0};$$

$$\langle \Delta C^2 \rangle = \frac{\langle I^2(\vec{\rho}, z_f) \rangle - \langle I(\vec{\rho}, z_f) \rangle^2}{I_0^2}, \quad (1)$$

where $\langle I(\vec{\rho}, z_f) \rangle$ is the time mean intensity, $\langle I^2(\vec{\rho}, z_f) \rangle$ is the time mean square intensity, I_0 is the time mean for background intensity, and $\vec{\rho}$ is the two-dimensional xy -position vector of a point at the cell plane. These operations can be readily performed using ImageJ¹⁸ and return an image representing the DMC and another representing the DMCF. At small defocusing distances, the DM contrast for an object with two diffracting surfaces is,⁹

$$C(\vec{\rho}, z_f) = \frac{\Delta n}{n_0} \{ [z_f - h_1(\vec{\rho})] \nabla^2 h_1(\vec{\rho}) + [z_f + |h_2(\vec{\rho})|] \nabla^2 |h_2(\vec{\rho})| \}, \quad (2)$$

where Δn is the refractive index difference between the cell and its surrounding solution and n_0 is the immersion oil refractive index. $h_1(\vec{\rho})$ and $h_2(\vec{\rho})$ are the height functions for upper and lower RBC surface membranes, respectively. This equation is valid at the linear region of $\langle C \rangle \times z_f$, limited to $z_f = \pm 2 \mu\text{m}$ for a red cell. Subtracting, pixel by pixel, the contrast images taken at $z_f = 0$ and $z_f = 2 \mu\text{m}$, we have

$$\langle C_{z_f=2 \mu\text{m}} \rangle - \langle C_{z_f=0 \mu\text{m}} \rangle = \frac{\Delta n}{n_0} (z_{f_2} - z_{f_0}) \nabla^2 H(\vec{\rho}), \quad (3)$$

where $H(\rho) = h_1(\rho) + |h_2(\rho)|$ is the cell thickness. Applying a Fourier transform to Eq. (3), dividing it by $-q^2$, and performing an inverse Fourier transform,⁹ we recovered the cells' thickness map

$$H = \frac{n_0}{\Delta n(z_{f_2} - z_{f_0})} \mathcal{F}^{-1} \left(\frac{\mathcal{F} \{ \langle C_2 \rangle - \langle C_0 \rangle \}}{-q^2} \right). \quad (4)$$

Multiplying the pixel area by the thickness value for each pixel, the sum of all multiplications returned the cell volume, such as $V = \sum_{\text{pixel}} A_{\text{pixel}} \times H_{\text{pixel}}$.

Using the cell thickness map $H(\vec{\rho})$ and defining $\delta(\vec{\rho}) = h_1(\vec{\rho}) - |h_2(\vec{\rho})|$ as the asymmetry between the RBC surface membranes, we have⁹

$$h_1(\vec{\rho}) = \frac{H(\vec{\rho}) + \delta(\vec{\rho})}{2};$$

$$h_2(\vec{\rho}) = \frac{-H(\vec{\rho}) + \delta(\vec{\rho})}{2}. \quad (5)$$

For $z_f = 0$, Eq. (2) can be rewritten as

$$\nabla^2 \delta + \frac{\nabla^2 H}{H} \delta = -\frac{2n_0}{\Delta n H} C(\vec{\rho}, 0), \quad (6)$$

which is a nonhomogeneous Helmholtz equation with variable coefficients. This equation can be solved numerically and once the asymmetry was determined the height profiles of the surface membranes were retrieved by means of Eq. (5). Using those profiles, the total 3-D image of the cell was formed.

Using Monge parametrization, the cell surface area was defined as

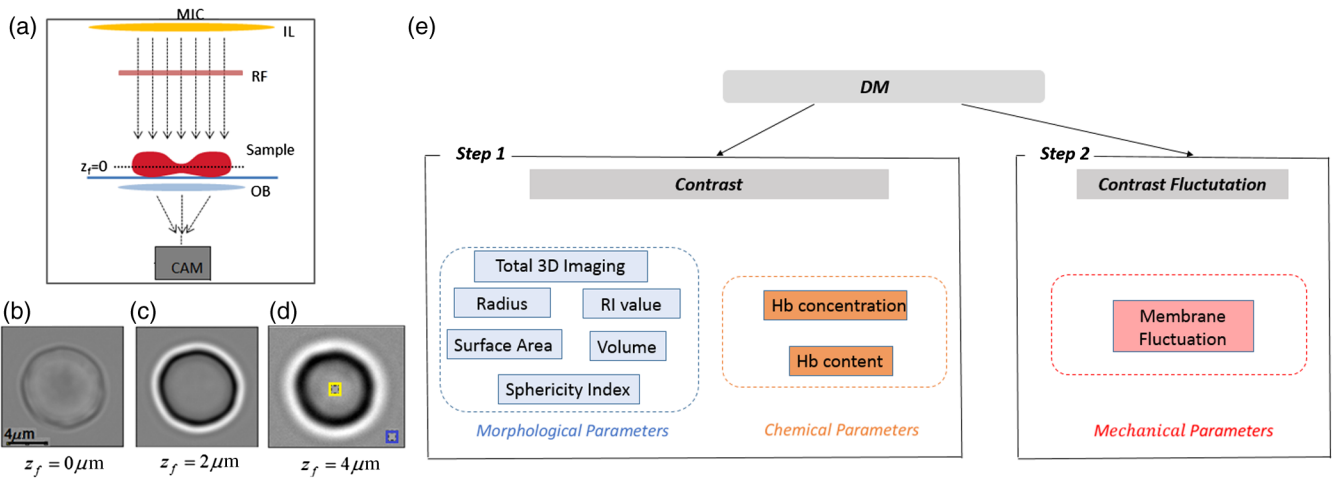


Fig. 1 (a) DM setup: inverted optical microscope operating in bright-field mode (MIC), halogen lamp (IL), long-pass filter (RF), objective (OB), and camera (CAM). The cell minimum contrast plane defines defocus position, $z_f = 0 \mu\text{m}$. (b)–(d) Image of a red cell in three different defocus positions (z_f) corresponding to $z_f = 0, 2,$ and $4 \mu\text{m}$, respectively. (d) The central square indicates the region where the cell contrast fluctuation was measured and the other square points out the background region considered. (e) Schematic fluxogram of the analysis that retrieves the parameters for single RBCs using DM.

$$A = \int \sqrt{1 + \left(\frac{\partial h_{1/2}}{\partial x}\right)^2 + \left(\frac{\partial h_{1/2}}{\partial y}\right)^2} dx dy, \quad (7)$$

and the SI was calculated as $4.84V^{2/3}/A$.

The Hb concentration for individual RBCs was estimated by means of its known relation with refractive index:¹⁹⁻²¹

$$n_{\text{Hb}} = n_{\text{H}_2\text{O}} + \alpha(\lambda)C_{\text{Hb}}, \quad (8)$$

where n_{Hb} is the Hb refraction index, $\alpha(\lambda)$ is the refraction increment (in dL/g), and C is the Hb concentration (in g/dL). The value of the increment coefficient used was 0.002 dL/g at $\lambda = 650$ nm.²² The RBC refractive indexes (n_{RBC}) for 250, 350, and 450 mOsm/kg were calculated by an extrapolation from data previously obtained for 200, 300, and 400 mOsm/kg.⁹ Finally, the cell Hb content (in pg) was given by multiplying the Hb concentration by the cell volume.

The DMCF for an object with two diffracting surfaces is,⁷

$$\begin{aligned} \langle \Delta C^2(\vec{\rho}) \rangle = & \frac{(\Delta n k_0)^2}{\pi} \int_{q_{\min}}^{q_{\max}} q dq \left\{ \langle |u_1(\vec{q})|^2 \rangle \right. \\ & \times \sin^2 \left[\frac{(z_f - h_1)q^2}{2k} \right] + \langle |u_2(\vec{q})|^2 \rangle \\ & \left. \times \sin^2 \left[\frac{(z_f - h_2)q^2}{2k} \right] \right\}, \quad (9) \end{aligned}$$

where the terms $\langle |u^2(\vec{q})|^2 \rangle$ are the membranes fluctuation spectra and $k = n_0 k_0$, and k_0 is the illumination light wavenumber in vacuum. In the asymptotic limit ($z_f \rightarrow \infty$), Eq. (9) simplifies to

$$\langle \Delta C^2_{z_f \rightarrow \infty} \rangle = (\Delta n k_0)^2 \langle u^2 \rangle, \quad (10)$$

where $\langle u^2 \rangle$ is the amplitude of the height fluctuations of both surface membranes. In case of RBCs, the asymptotic limit is satisfied for $z_f > 3 \mu\text{m}$. Thus, to access RBC surface fluctuations, we measured $\langle (\Delta C)^2 \rangle$ at $z_f = 4 \mu\text{m}$, in a central area of $1.0 \times 1.0 \mu\text{m}^2$ of the cell [Fig. 1(d)], not influenced by diffraction. The camera noise was subtracted from DM contrast fluctuation data before determining $\langle u^2 \rangle$.

In Fig. 2, we show the representative image of a typical RBC immersed in solutions with different osmolalities and obtained by applying the total 3-D image methodology.⁹ Erythrocytes immersed in isotonic solutions [Fig. 2(c)] generally present a biconcave discoid shape, whereas in hypotonic solutions [Figs. 2(a) and 2(b)] the cells swell due to water influx and tend to lose the curved region at the center. In hypertonic solutions [Figs. 2(d)–2(f)], the cells shrink as a result of water efflux and hence display a more pronounced dimpled region at the center, with a smaller separation between the upper and lower surface membranes. DM axial resolution allows one to obtain images of the RBCs' surface membranes separated by a distance as small as 150 nm.⁹ One can also observe morphological differences between the upper and lower surface membranes, including the effects caused by the cell adhesion to the glass substrate. In Fig. 2(g), angular average of the height profiles of both upper and lower surfaces of the RBCs represented in (a), (c), and (f) are depicted.

Figure 3 presents the mean values for volume and surface area (a), radius and SI (b), Hb content and concentration (c), and mean amplitude membrane fluctuation (d) over 10 cells analyzed in each condition (200 to 450 mOsm/kg). As can be seen the mean surface area slightly changes as the osmolality of the solution varies, assuming values from 122 to 140 μm^2 . Differently, the mean volume tends to decrease as the solution osmolality increases, from 90 to 80 μm^3 , and gradually increases for smaller osmolalities, from 90 to 120 μm^3 .

An important index related to cell morphology is the SI, which describes how similar the cell shape is to a sphere. The SI for a typical RBC is 0.7. As shown in plot (b) of Fig. 3, when immersed in hypotonic solutions, the cells' SI rise considerably, assuming values close to 1, which implies that the cell shape is nearly a sphere. This value also indicates an increase in membrane tension, here caused by cell swelling. Another important aspect monitored by DM methodologies is the cell radius. From Fig. 3(b), it is easy to notice a reduction in RBC radius as the solution osmolality is decreased and a minor growth to higher osmolalities. An analysis of the Hb content in cells subjected to different osmolalities is seen in Fig. 3(c). The plot shows that the Hb content is constant for all osmolalities used, slightly varying around 30 pg. Moreover,

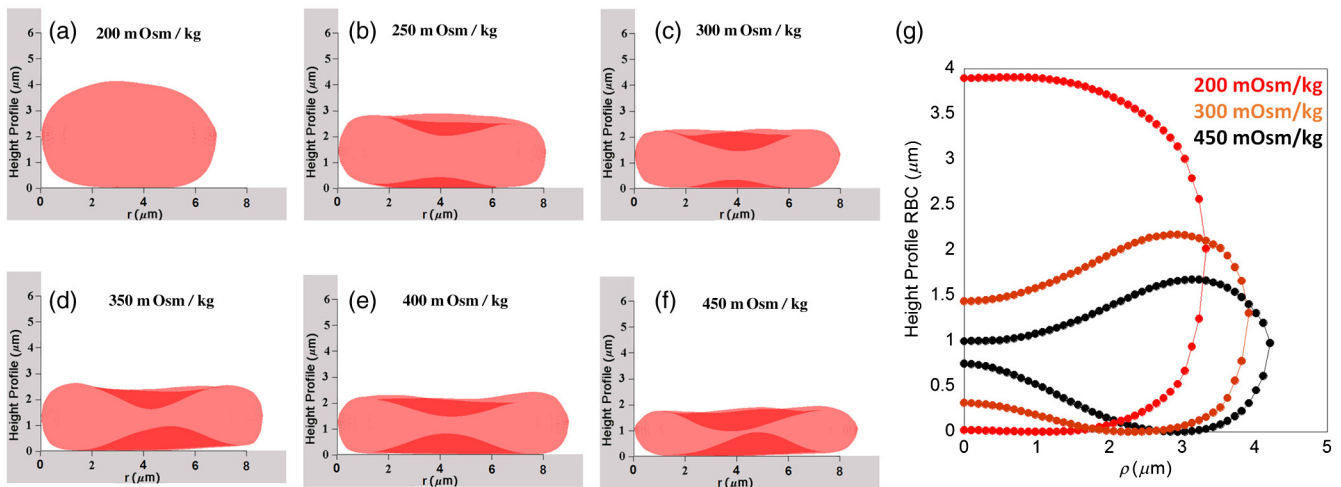


Fig. 2 (a)–(f) Total 3-D images of RBCs immersed in solutions with different osmolalities. (g) Height profiles of both upper and lower surface membranes red cells in (a), (c), and (f).

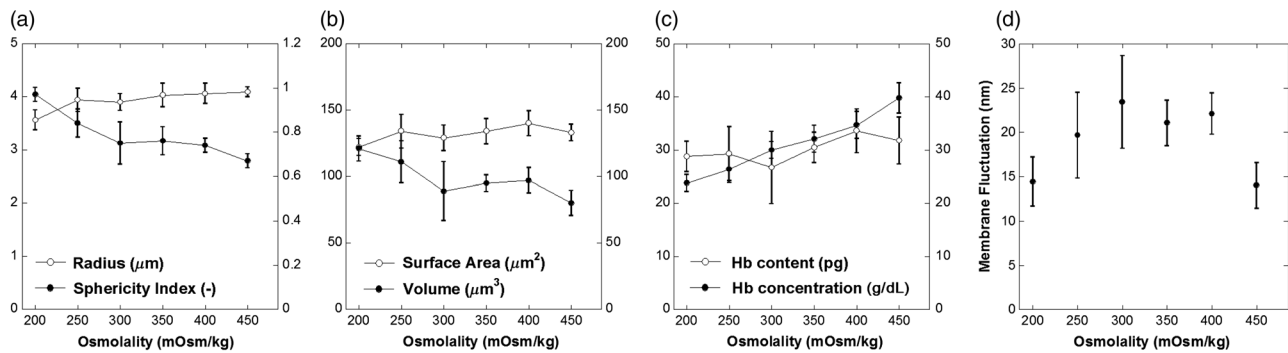


Fig. 3 (a) Mean surface area (open symbols) and volume (close symbols) at different osmolalities; (b) radius (open symbols) and Slex (close symbols); (c) Hb content (open symbols) and concentration (close symbols); and (d) amplitude of membrane fluctuation of both surface membranes. The symbols represent the mean values over 10 RBCs and error bars represent the standard deviation.

the Hb concentration data demonstrate an increasing monotonic behavior.

Finally, to obtain information over RBC deformability under different osmolalities, we measured membrane fluctuations using DM.^{4-7,10} Figure 3(d) presents the mean amplitude of both membrane fluctuations ($\sqrt{\langle u^2 \rangle}$) as a function of the solution osmolality. As shown in the plot, the maximum amplitude occurs at 300 mOsm/kg and all deviations from this osmolality induce a decrease in membrane fluctuation amplitude. These results indicate a decrease in RBC deformability in both hypo and hypertonic conditions.

This work uses DM methods for the profiling of RBCs under different osmotic conditions. Compared with other QPI techniques, DM benefits from operating with a commercial bright-field microscope and white light illumination, conferring stability and spatial uniformity, and thus being easier to implement. All presented measurements can be performed in a short period of time and only require images taken at three different focal positions. In that sense, DM methods point out to a new and practical way of exploring possible indicators for hemodiagnosis.

Acknowledgments

We would like to acknowledge the financial support from the Brazilian Agencies CNPq, CAPES, FAPEMIG, PRONEX-FAPEMIG, and Instituto Nacional de Fluidos Complexos e Aplicações (INFCx).

References

1. M. Diez-Silva et al., "Shape and biomechanical characteristics of human red blood cells in health and disease," *MRS Bull.* **35**(5), 382–388 (2010).
2. Y. Kim, K. Kim, and Y. Park, "Measurement techniques for red blood cell deformability: recent advances," in *Blood Cell—An Overview of Studies in Hematology*, T. E. Moschandrou, Ed., pp. 167–194, InTech (2012).
3. K. Youngchan, "Profiling individual human red blood cells using common-path diffraction optical tomography," *Sci. Rep.* **4**, 6659 (2014).
4. U. Agero et al., "Cell surface fluctuations studied with defocusing microscopy," *Phys. Rev. E* **67**(5), 051904 (2003).

5. L. G. Mesquita et al., "Defocusing microscopy: an approach to red blood cell optics," *Appl. Phys. Lett.* **88**, 133901 (2006).
6. J. C. Neto et al., "Measuring optical and mechanical properties of living cells with defocusing microscopy," *Biophys. J.* **91**, 1108–1115 (2006).
7. G. Glionna et al., "Tomography of biological interfaces using defocusing microscopy," *Appl. Phys. Lett.* **94**, 193701 (2009).
8. B. Hissa et al., "Membrane cholesterol removal changes mechanical properties of cells and induces secretion of a specific pool of lysosomes," *PLoS One* **8**, e82988 (2013).
9. P. M. S. Roma et al., "Total three-dimensional imaging of phase objects using defocusing microscopy: application to red blood cells," *Appl. Phys. Lett.* **104**, 251107 (2014).
10. S. Etcheverry et al., "Real-time study of shape and thermal fluctuations in the echinocyte transformation using defocusing microscopy," *J. Biomed. Opt.* **17**(10), 106013 (2012).
11. T. E. Gureyev and K. A. Nugent, "Rapid quantitative phase imaging using the transport of intensity equation," *Opt. Commun.* **133**, 339–346 (1997).
12. D. Paganin and K. A. Nugent, "Noninterferometric phase imaging with partially coherent light," *Phys. Rev. Lett.* **80**, 2586–2589 (1998).
13. T. J. Smart et al., "A study of red blood cell deformability in diabetic retinopathy using optical tweezers," *Proc. SPIE* **9548**, 954825 (2015).
14. R. Agrawal et al., "Red blood cells in retinal vascular disorders," *Rev. Sci. Instrum.* **561**, 53–61 (2016).
15. M. Suwalsky et al., "Effects and antioxidant capacity of *Solanum crispum* (Natre) in vitro assayed on human erythrocytes," *J. Membr. Biol.* **249**(3), 349–361 (2016).
16. I. Castillo et al., "Structural and functional effects of benzimidazole/thioether-copper complexes with antitumor activity on cell membranes and molecular models," *J. Inorg. Biochem.* **156**, 98–104 (2016).
17. H. P. Berlien and G. J. Muller, *Applied Laser Medicine*, Springer, Germany (2003).
18. C. A. Schneider et al., "NIH Image to ImageJ: 25 years of image analysis," *Nat. Methods* **9**, 671–675 (2012).
19. R. Barer, "Interference microscopy and mass determination," *Nature* **169**, 366–367 (1952).
20. G. Popescu et al., "Optical imaging of cell mass and growth dynamics," *AJP Cell Physiol.* **295**(2), C538–C544 (2008).
21. K. G. Phillips et al., "Measurement of single cell refractive index, dry mass, volume, and density using a transillumination microscope," *Phys. Rev. Lett.* **109**(11), 118105 (2012).
22. A. I. Yusipovich et al., "Laser interference microscopy in erythrocyte study," *J. Appl. Phys.* **105**, 102037 (2009).